AIAA JOURNAL
Vol. 30, No. 5, May 1992

# Unsteady Flow Past an Airfoil Pitching at a Constant Rate

C. Shih,* L. Lourenco,† L. Van Dommelen,† and A. Krothapalli‡
*Florida A & M University and Florida State University, Tallahassee, Florida 32316*

**The unsteady flow past a NACA 0012 airfoil in pitching-up motion is experimentally investigated in a water towing tank using the particle image displacement velocimetry (PIDV) technique. The Reynolds number, based on the airfoil chord and the freestream velocity, is 5000. The airfoil pitching motion is from 0 to 30 deg angle of attack at a dimensionless pitch rate $\dot{\alpha}$ of 0.131. Instantaneous velocity fields at different times have been acquired over the entire flowfield. Using the whole-field data, the out-of-plane component of vorticity is computed. The following features are observed. Boundary-layer separation near the airfoil leading edge leads to the formation of a vortical structure. The evolution of this vortex along the upper surface dominates the aerodynamic performance of the airfoil. Complete stall emerges when the boundary layer near the leading edge detaches from the airfoil, under the influence of the vortex. The vortex further triggers the shedding of a counter-rotating vortex near the trailing edge. A parallel computational study using the discrete vortex, random walk approximation has also been conducted. In general, the computational results agree very well with the experiment.**

## Introduction

INCREASED interest in improving the maneuverability of fighter aircraft has resulted in significant changes in the required aerodynamic performance. This increased aerodynamic performance is only possible if new designs take full advantage of unsteady aerodynamic effects such as dynamic stall. However, a complete understanding of these complex unsteady effects has not yet been achieved, and there is a great need for systematic fundamental studies. The difficulty mainly arises because these flows are extremely complex and are not amenable to standard experimental and numerical techniques. The level of understanding needs to advance from qualitative conjectures based on flow visualization and/or the measurement of global quantities, such as $C_L$, $C_D$, and $C_M$, to the quantitative measurement of the instantaneous flowfield during the various stages of the dynamic stall process, as well as to the simultaneous development of mathematical models that incorporate all of the important physical effects. For example, a prominent feature about the flow past a pitching airfoil is the emergence of large-scale vortical structures when the flow separates from the airfoil surface. The temporal and spatial evolution of these structures dominates the unsteady flow behavior over the airfoil. They can induce considerable lift increase or trigger a catastrophic flow breakdown when they detach from the surface.[1-4] Consequently, to predict and eventually control the aerodynamic performance of a pitching airfoil, understanding of the unsteady characteristics of the vortices from a fundamental, fluid mechanical viewpoint is imperative.

To understand the dynamical behavior of these vortices and their interactions with the lifting surface, it is necessary to study the spatial vorticity distribution at each instant. This immediately excludes the use of traditional single-point velocity measurement techniques, such as hot-wire anemometry or laser Doppler anemometry (LDA). In view of this, a new experimental technique, particle image displacement velocimetry (PIDV), has been developed in our laboratory. This technique can provide the instantaneous two-dimensional velocity field in a selected plane of the flowfield with sufficient spatial accuracy, from which the instantaneous vorticity field can be obtained. The detailed description of the technique is given by Lourenco and Krothapalli.[5]

A comparative numerical study is also carried out with a computer simulation of the Navier-Stokes equations using a fast, discrete vortex, random walk scheme.[6,7] It will be shown that the global flow features predicted by the computation compare well with the experiment.

The main parameters of the problem are the Reynolds number $R_e$, the nondimensionalized pitch rate $\dot{\alpha}$, which is normalized with the airfoil chord and freestream velocity, the maximum angle of attack, and the geometry of the airfoil. The Reynolds number, based on the airfoil chord and the freestream velocity, is 5000 both for the experiment and for the computation. Although the Reynolds number is too low for many practical applications, it is more accurately represented numerically and experimentally, hence leading to a clear picture of the flow evolution. Whether the evolution would be significantly affected by the Reynolds number is currently unknown; it is known that the location and time of the initial boundary-layer breakup are asymptotically independent of the Reynolds number.[6] Experiments that involve much higher Reynolds numbers are currently being conducted in our laboratory. The airfoil pitches up from zero angle of attack to 30 deg at a pitch rate of $\dot{\alpha} = \omega c/U_\infty = 0.131$. In other words, the airfoil completes its 30-deg pitching motion in about four chord-length travel. As airfoil shape, a NACA 0012 profile was selected.

## Particle Image Displacement Velocimetry

The operation of the PIDV technique involves the illumination of the flow, seeded with small tracer particles, with a thin laser light sheet. The light scattered by the seeding particles, which follow the local fluid motion, generates a moving particle-image pattern. This pattern is recorded using a multiple exposure photographic technique, the distance between corresponding particle images being proportional to the local displacement. Optical and digital image processing techniques are used to convert this information into local velocity data. This process uses a focused laser beam to interrogate a small area of the multiple exposed photographic film. The diffraction pattern produced by the coherent illumination of the multiple images in the photographic transparency generates Young's fringes, in the Fourier plane of a lens, if the multiple

Received May 15, 1991; revision received Aug. 7, 1991; accepted for publication Aug. 21, 1991. 

*Assistant Professor, FAMU/FSU College of Engineering, P.O. Box 2175. Member AIAA.
†Associate Professor, FAMU/FSU College of Engineering, P.O. Box 2175. Member AIAA.
‡Professor, FAMU/FSU College of Engineering, P.O. Box 2175. Member AIAA.

particle images within the interrogating area correlate. These fringes have an orientation that is perpendicular to the direction of the local displacement and a spacing inversely proportional to the displacement. A fully automated process has been devised to digitize and process the fringe images (see Ref. 5 for details).

One limitation of the basic PIDV method is that it is not possible to determine the direction of the velocity vector. Thus it is difficult to discriminate against the directional ambiguity that the possible reversing motion in the flowfield introduces. To resolve this problem, a "velocity bias technique" has been used.[5] A uniform reference motion is added to the flow, thus superposing a velocity shift to the real flowfield. A properly chosen shift can insure that all image displacements occur in the same direction, thereby eliminating the ambiguity. The true flowfield can be recovered later by removing this artificial shift from the raw velocity data. In this work, a rotating mirror was used to produce the image shift.

A dual pulsed laser system, consisting of two Spectra-Physics DCR-11 Nd-Yag pulsed laser systems, is used to provide the double illumination pulses. A system of prisms and polarizing cube beam combiners make the light beams emitted from the two lasers colinear; see Fig. 1a. Time separation between the laser light pulses can be varied from a fraction of 1 $\mu$s to a few seconds by adjusting a pulse generator used as a trigger. A cylindrical lens is used to form the combined beam into a laser sheet that illuminates the midspan section of the airfoil. Metallic coated particles (TSI model 10087), with an average diameter of 11 $\mu$m, are used as the flow tracers. A phase-triggered 35-mm camera (Nikon F-3) is used in the recording of the flowfield. Synchronization between components is accomplished using a Tektronix modular electronics system. This system also provides the phase reference between the motion of the airfoil and the PIDV photographic timing sequence.

## Experimental Facility

The experiments were performed in a towing water tank facility, which is 180 cm long and 43 by 55 cm in cross-sectional area. A dc servo motor with a towing speed varying from 0.3 to 30 cm/s drives the towing carriage. A NACA 0012 airfoil with a chord length of 6 cm and an aspect ratio of 6.67 is used. The camera and the scanning mirror system are mounted on a reinforced, vibration-free platform that extends from the airfoil carriage. A motor speed control system controls the towing speed via a digital-to-analog converter. To insure a smooth traverse of the towing carriage, an acceleration ramp at the beginning of the travel and a deceleration ramp at the end of the travel are implemented on the controller. The airfoil pitching motion is provided by a stepping motor with a programmable controller, which is preprogrammed with the test profile and activated by the host computer. The airfoil angle changes linearly from 0 to 30 deg after the airfoil is towed more than one chord length. A DEC Vaxstation II computer monitors all motions; see Fig. 1b.

## Numerical Simulation Scheme

A numerical study using a random walk vortex simulation of the full Navier-Stokes equations was performed. In these computations, the vorticity field was represented by discrete vortex blobs, and the diffusion processes were simulated by adding a random component of magnitude $\sqrt{2\nu\Delta t}$ to the vortex motion.

Using this method, no accuracy is lost in describing the strong convection processes that are typical of unsteady separated flows because there are no spatial convective terms to be differenced. Additionally, the computational domain is truly infinite without any artificial boundary conditions. But most importantly, since the computational elements are only used in the limited regions containing appreciable vorticity, the resolution (the smallest scales that the computation can distinguish), is high.

On the other hand, for this type of statistical method, the accuracy is not very high. Fortunately, the fast solution-adaptive Laurent series technique[7] allows a large number of vortex blobs to be included, up to 32,000, while retaining the high resolution of the individual vortices and the infinite domain. An earlier investigation[6] of flows about circular cylinders at Reynolds numbers of 550 and 10,000 showed very good agreement with established two-dimensional Navier-Stokes and experimental results, but with typical random fluctuations of about 10%.

The boundary condition on the normal component of the velocity at the airfoil surface was satisfied by mirror vortices, after the airfoil was mapped onto a circle. The mapping used was a generalized Von Mises transform that exactly reproduces the slightly blunted trailing edge of the NACA 0012.

The no-slip boundary condition was satisfied by the addition of vortices at the wall during each time step. To do this, first all the vortices within a distance from the wall equal to 1.27 times the random step size were removed. Then a ring of new vortices was added at a distance from the wall equal to 0.675 times the random step to correct the wall slip to zero. (The distance for adding vortices equals the mean diffusion distance during one time step of vorticity generated at the wall; the removal distance was chosen based on a statistical study requiring that the scheme handles locally uniform vorticity distributions accurately, not unlike discretization techniques in finite difference procedures.) The vortex diameter was chosen to be 0.675 times the random step; testing showed that the results depended little on the actual value used. This procedure of satisfying the no-slip condition has some similarities to one recently proposed by Smith and Stansby,[8] but here the vortices are initially placed at a deterministic location.

To allow for the pitching motion, the equations for the vortex motion were developed in an inertial reference frame and subsequently converted to an airfoil-based system. This is required since Kelvin's theorem cannot be used in a rotating

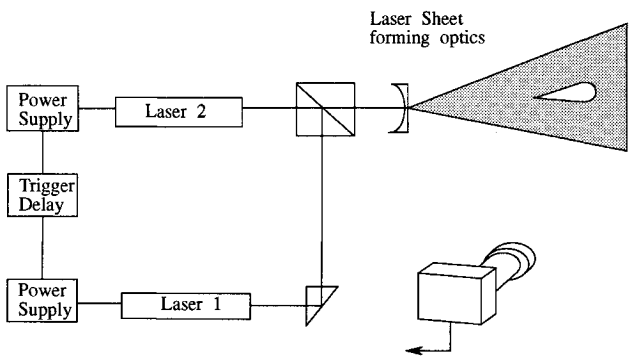


a) dual-pulsed laser system

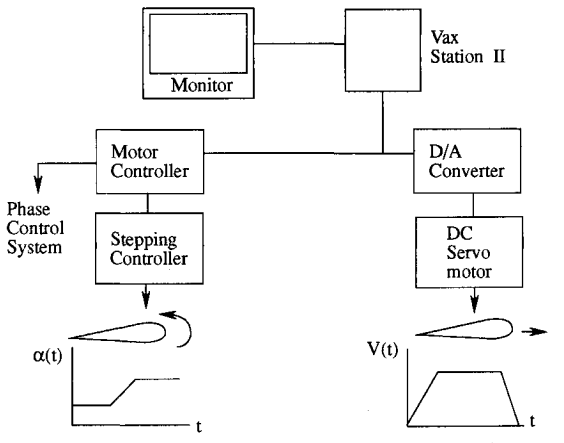


b) the airfoil's motion control system

**Fig. 1 Schematic of experimental setup.**

coordinate system. The force on the airfoil is determined by differentiating an integral of the vorticity distribution, rather than directly from the wall shear and pressure.[9] The computation was performed initially using a CYBER 205 and later an ETA 10 computer. The results were postprocessed on a MicroVax II computer, at which time a fast Fourier transform technique was used to find the streamlines.

In the form described, the vortex method is essentially free of adjustable parameters. Although no high accuracy is claimed, previous comparisons with established computational and experimental results for the circular cylinder showed quite good agreement.[6] At higher Reynolds numbers, the method could also describe very fine scales in the vortex formation process. For the airfoil, the results appeared to agree well with the experimental data.

## Results and Discussion

### Experimental Accuracy and Restrictions

The experimental velocity data were acquired by point-wise scanning of the film transparencies following a Cartesian grid. The step size of the scanning operation was chosen to be 0.5 mm in both directions; the corresponding step size in the physical plane is 1.25 mm. The interrogation beam diameter corresponds to an equivalent physical probe size of 0.625 mm, which is approximately half the mesh size. The Young's fringes produced by the beam were digitally processed to produce the velocity at the interrogated point on the negative, and the vorticity was found by numerical differentiation.

The overall accuracy of the measurement has been calibrated by examination of the uniform velocity field created by towing the camera carriage system at a known constant speed, and the velocity is found to be accurate to within 1%. Vorticity values are obtained by centrally differentiating the velocity field. These values are expected to be within 5% accuracy.

Because of the blockage of the laser sheet by the airfoil model, no data were obtained below the airfoil. If the total flowfield is needed, this inconvenience can be easily removed; for example, a reflecting mirror can be used to redirect the laser light sheet below the airfoil. The boundary-layer flow very close to the airfoil surface is not included in this experiment, since we are primarily interested in the study of the global features of the flowfield. However, a new set of experiments and associated numerical simulations have already been initiated that focus specifically on the behavior of the boundary flow close to the surface. Possibly these can provide a better physical understanding of the unsteady vortex formation process.

### Global Flow Description

As mentioned earlier, the airfoil is started with a ramp-type motion at zero angle of attack and is allowed to move one chord length, after which the flowfield is fully established with very minimal effects of the starting process. Next the airfoil is impulsively given its pitching motion and allowed to pitch to 30 deg angle of attack. During the pitch-up motion, the airfoil travels approximately four chord lengths. Once the pitch-up motion stops, the airfoil is allowed to travel an additional four chord lengths before it comes to a complete stop. In the present experiments, the airfoil pitches about its quarter chord point.

Figures 2 and 3 show the time development of the flow around the pitching airfoil obtained using the PIDV technique. It is important to point out that no phase-averaging technique was used. Such averaging tends to significantly

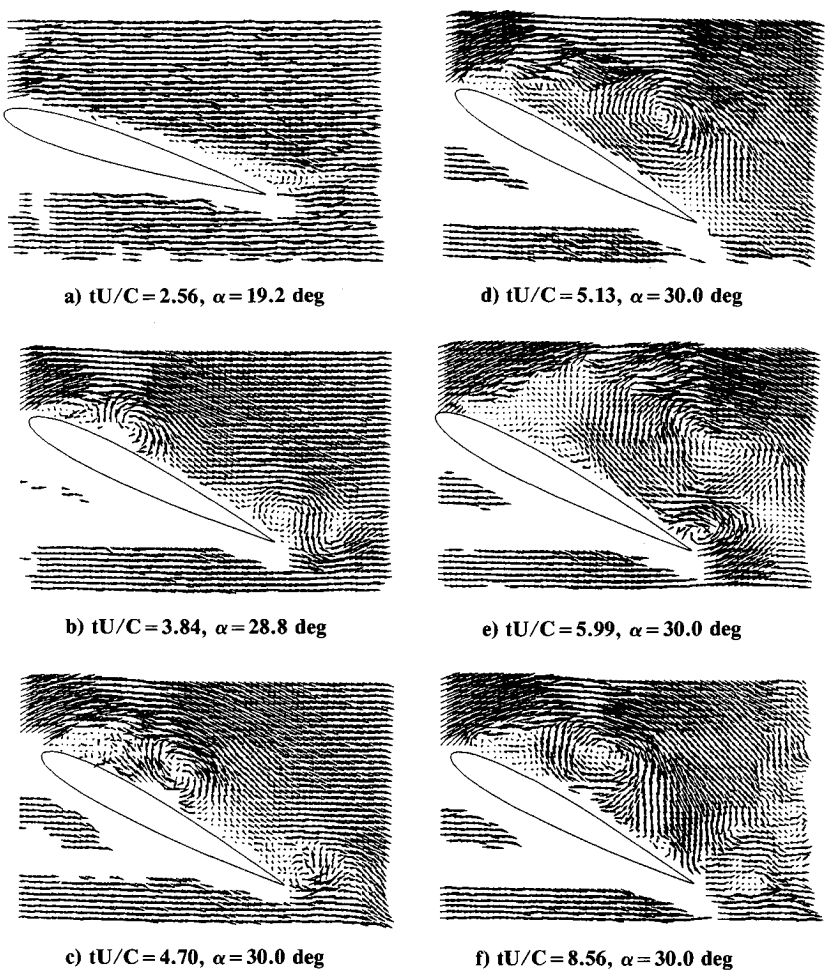

a) tU/C = 2.56, $\alpha$ = 19.2 deg

d) tU/C = 5.13, $\alpha$ = 30.0 deg

b) tU/C = 3.84, $\alpha$ = 28.8 deg

e) tU/C = 5.99, $\alpha$ = 30.0 deg

c) tU/C = 4.70, $\alpha$ = 30.0 deg

f) tU/C = 8.56, $\alpha$ = 30.0 deg

**Fig. 2 Time development of the instantaneous velocity field measured by particle image displacement velocimetry technique.**

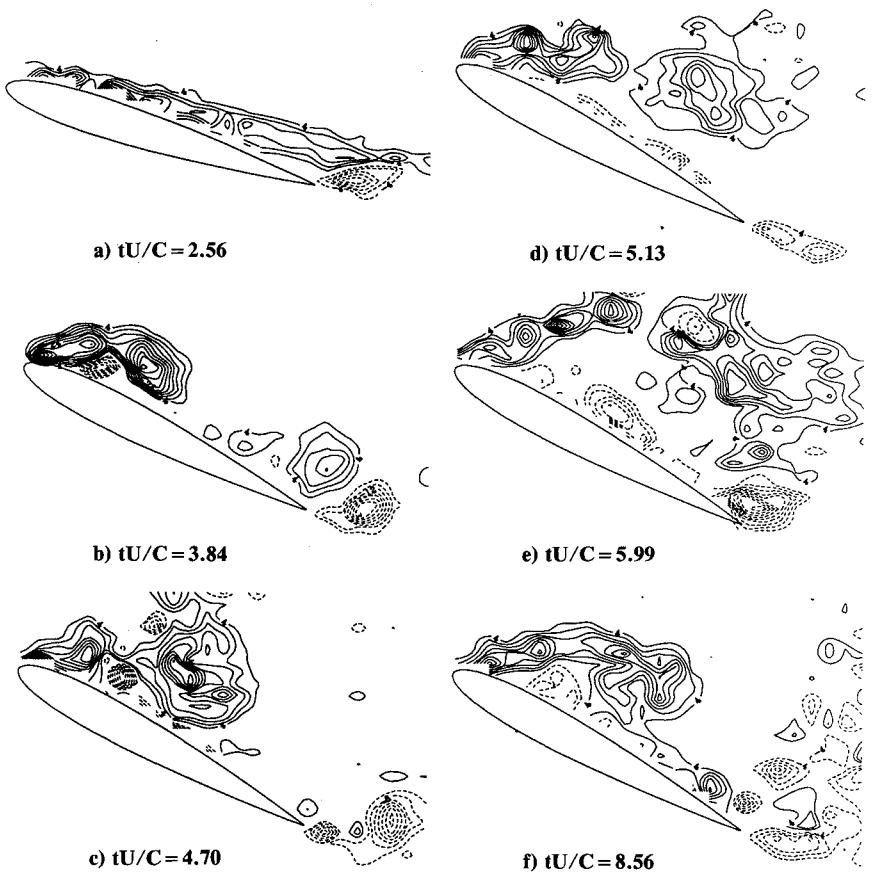


**Fig. 3 Time development of the instantaneous vorticity field measured by particle image displacement velocimetry technique.**

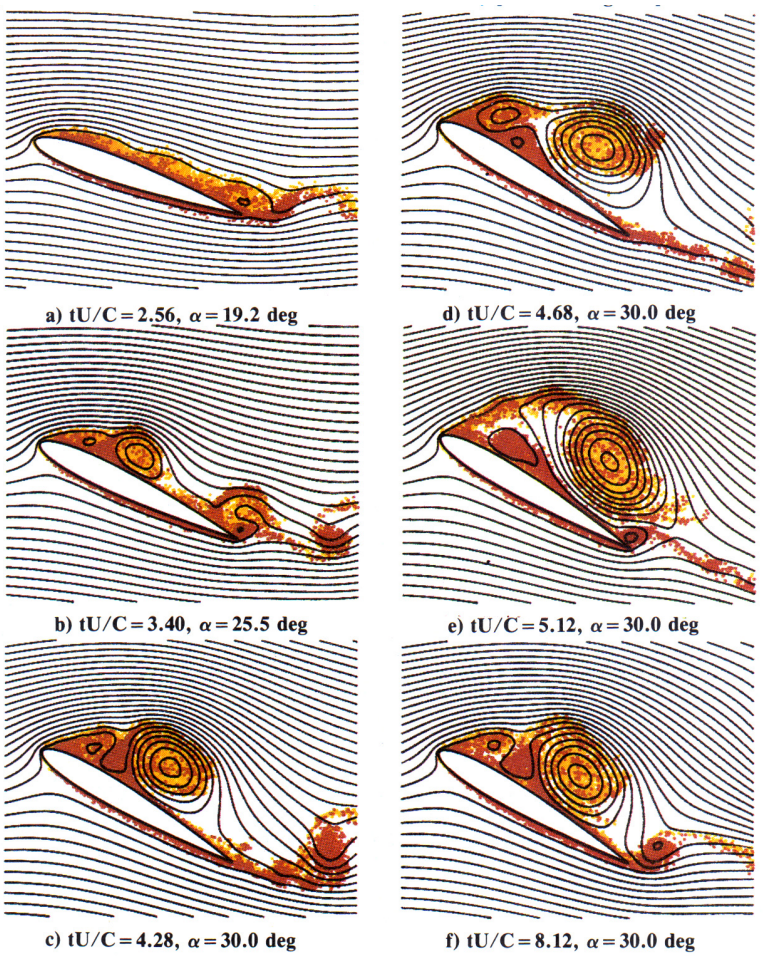


**Fig. 4 Computational results of the instantaneous streamline pattern and the distribution of discrete vortices.**

"smear out" delicate features such as thin vortex sheets and such; and we believe that fundamental understanding of transient phenomena requires the realization that the flow is not a featureless average but is built from sharply defined features. All experimental results presented in this paper are instantaneous information acquired during the same experimental run. Figure 2 presents the velocity field at different times as uniformly scaled velocity vectors. The corresponding vorticity fields are presented as isovorticity contour plots in Fig. 3.

These experimental data can be compared with the results of the random walk vortex simulation presented in Fig. 4. That figure shows both the instantaneous streamlines and the discrete vortices, with clockwise rotating vortices displayed in yellow and counterclockwise ones in red. The strength of the vorticity can approximately be related to the local concentration of the corresponding color at that region.

Based on these figures and other observations by the authors and others,[3,4,10] the unsteady flow development over the pitching airfoil can be classified into successive stages as follows.

*Vortex Formation Stage*

Shortly after the beginning of the pitching motion, but not until the airfoil pitches well beyond the 12-deg static stall angle, a flow reversal near the trailing edge can be identified by the presence of counter-rotating (red) vortices at the surface. Similar to steady trailing-edge stall, the reversed flow region expands upstream toward the leading edge; see Fig. 4a. However, unlike for steady flow, for the unsteady case, flow reversal does not necessarily imply a significant departure of the boundary layer from the wall.[11,12] Thus, while the boundary layer on the rear portion of the airfoil thickens, the airfoil flow seems to remain mostly attached. This is presumably a finite Reynolds number effect; for sufficiently high Reynolds number we expect at least some trailing edge separation for all times.[13]

Because of the pitch-up motion, the lower surface continuously sheds counterclockwise vorticity that rolls up into the familiar starting vortex.[14] This vortex tends to accelerate the downstream convection process along the upper surface and some local accumulation occurs near the trailing edge. Meanwhile the first evidence of the formation of a leading-edge vortex begins to develop in the form of a local thickening of the boundary layer. A result of these effects is that the upper surface vorticity downstream of the leading-edge vortex assumes an individualized appearance known as the "shear layer vortex"[10]; see Figs. 3a and 4a.

As a first step towards individualizing into a true leading-edge vortex, the boundary-layer flow near the nose separates by means of local thickening of the boundary layer with the general appearance of the asymptotic structure given in Fig. 2 of Van Dommelen and Cowley.[15] That structure is believed to be generally valid for unsteady separation; like some other boundary-layer structures, this one is conventionally known by the names of the authors who first described it as the Van Dommelen and Shen singularity; we will follow this terminology here. A brief description of the structure is given later. Because of the separation process, the upper part of the boundary layer forms a "free" shear layer, as has also been pointed out by, e.g., Tietjens,[16] and Visbal,[2] and Visbal and Shang.[10] This shear layer "rolls up" into an individualized vortex, in a mechanism resembling Kelvin-Helmholtz instability. This vortex, the dynamic-leading-edge-stall or primary vortex, initially remains close to the surface.

*Vortex Convection Stage*

While the primary vortex is moving along the surface, it interacts with the local boundary-layer fluid below and induces an upstream accumulation and eruption of reversed boundary-layer vorticity. The reversed vorticity interacts with vorticity arriving from the leading edge to form a counter-rotating vortex pair. Harvey and Perry[17] and Didden and Ho[18] have observed similar phenomena. The reversed leading-edge vortex seems to induce the primary vortex upward away from the surface where it encounters a faster convection velocity and moves more rapidly downstream; see Figs. 2b, 3b, and 4b.

In the meantime, the shear-layer vortex at the upper surface near the trailing edge increases the shedding of reversed lower surface vorticity from the trailing edge. The shear-layer vortex interacts with this reversed trailing-edge vortex so that a second pair of counter-rotating vortices is formed at the trailing edge.

The leading-edge vortex continues to grow and convect downstream. Behind this primary vortex, the leading-edge boundary-layer vorticity continues to be shed, and the interactions between this vorticity, the reversed leading-edge vortex, and the primary dynamic-stall vortex appear to play an important role in the development of the unsteady flow characteristics. For example, at $tU/C = 4.7$, as shown by Figs. 2c and 3c, an upstream vortex seems to merge with the major vortex, resulting in an apparent slowdown of the position of the latter if evaluated in the manner of Fig. 5.

A measure of the convection of the primary leading-edge-stall vortex along the upper surface is obtained by choosing the position of this vortex as the centroid of the vorticity capacity carried by it. The centroid is defined as

$$x_c = \frac{1}{\Gamma}\int\int x\omega \, dx \, dy \tag{1}$$

$$y_c = \frac{1}{\Gamma}\int\int y\omega \, dx \, dy \tag{2}$$

where

$$\Gamma = \oint \boldsymbol{u} \cdot d\ell = \int\int \omega \, dx \, dy \tag{3}$$

The domain of integration is designated somewhat subjectively by confining it to an area that surrounds the vortex. The threshold vorticity level of the integration domain is chosen as 10% of the maximum vorticity. The calculated centroid locations show negligible change as the threshold level varies from 10 to 30%. Figure 5 shows the time evolution for $x_c$, using the leading edge as reference point, as the vortex convects downstream. The vertical displacement $y_c$ varies by an insignificant amount, so it has been omitted from the figure. The motion appears to evolve in a stepwise pattern. After the ejection of the primary vortex at the leading edge, initially it convects steadily downstream. But between $tU/C = 4.27$ and 4.7, an amalgamation process develops between the primary vortex and a leading-edge vortex trailing behind it. This process is similar in appearance to the vortex merging process observed in a free shear layer, and the vortex convection defined by Fig. 5 is temporarily interrupted as indicated by the first leveled region on the curve. Downstream travel resumes immediately after completion of the merging. A second retardation of the position defined by Fig. 5 occurs between $tU/C = 5.13$ and 5.56. Interaction with the trailing edge is considered responsible for this slowdown. Finally, the convection process resumes a speed of 39% of the freestream velocity.

*Stall Onset Stage*

The downstream moving primary vortex induces a counter-rotating trailing-edge vortex that acts to increase the circulation around the airfoil; see Figs. 2e, 3e, and 4e. However, the trailing-edge vortex is still too close to the airfoil to increase the lift appreciably. Instead the lift drops off rapidly, indicated by computational results that have not been presented here, as the leading-edge boundary layer detaches completely from the wall and the leading-edge flow no longer follows the shape of the wall. These pictures suggest that ambient irrotational fluid entrained by the main vortex may play a role in causing the detachment of the leading-edge boundary layer; at least the irrotational region below the primary vortex in

Fig. 4e seems to expand rapidly as the vortex approaches the trailing edge of the airfoil.

*Stalled Stage*

During stall, the leading-edge boundary layer assumes, approximately, a 45-deg angle with respect to the chord line. A nearly stagnant region can be observed right under the shear layer near the front section of the airfoil. Yet the decrease in circulation around the airfoil decreases the rate of flow around the nose required for attached flow. Consistent with this, it is observed that the separated leading-edge vortex sheet is being washed downstream; see Figs. 2f, 3f, and 4f. As a result, the flow starts to follow the nose shape again, and the lift begins to pick up. But the increased circulation increases the flow around the nose, and the reattached flow will break away again shortly after, triggering another stall. The sequence of reattachment and breakdown cycles continues until it relaxes to a state consistent with static stall.

Direct comparison of the vorticity distributions of the experiments and the numerical simulation is not possible due to the singular nature of the discrete vortex method. Instead, global features are compared by examining the total circulation above the upper surface, defined as

$$\Gamma_u = \iint_{\text{upper}} \omega \, dx \, dy = \int_{\text{LE}}^{\infty} v \, dy + \int_{\text{LE}}^{\text{TE}} u \, dx + \int_{\infty}^{\text{TE}} v \, dy \qquad (4)$$

where LE and TE represent the leading and trailing edges of the airfoil, respectively. The circulation is normalized with the freestream velocity and the airfoil chord.

Figure 6 shows that the upper surface circulation predicted by the numerical simulation is consistently higher before stall and takes a much lower value during stall. The maximum circulation is 16% higher than the experimental data. The general trend agrees well between the two methods, with the computational results taking a small phase lead, $\Delta tU/C \approx 0.4$. The sections on reproducibility and on experimental accuracy give some possible reasons for these discrepancies.

**Van Dommelen and Shen Concept**

The Van Dommelen and Shen structure describes the initial breakup of unsteady boundary layers through a particle deformation that causes a significant thickening of the boundary layer. Before this structure can form, first reversed flow, in the form of a recirculation eddy, must occur. Next in the reversed flow region, a streamwise accumulation of fluid leads to a local thickening layer of fluid around the position of vorticity reversal. This local thickening layer of fluid in the middle of the boundary layer propels the top part of the boundary layer away from the wall. More precisely, the main part of the boundary layer in which the vorticity has the usual sense of rotation is ejected upward, whereas a layer of reversed vorticity remains immediately adjacent to the wall. The ejected main boundary layer takes the appearance of a free vortex sheet with a shape shown in Fig. 2 of Van Dommelen and Cowley.[15] The streamwise length scale of the shape of the free vortex layer is short compared with the chord, whereas its penetration away from the wall is large compared with the base boundary-layer thickness, consistent with a Kelvin-Helmholtz type evolution into one or more individualized vortices.[16]

The subsequent evolution of this individualized vortex layer can probably best be described in terms of the vorticity balance concept proposed by Reynolds and Carr.[19] Yet it is uncertain whether it will still be feasible to readily influence the flow once the vortex has individualized. It seems possible that the stage most accessible to manipulation would be the earlier development described by the Van Dommelen and Shen process.

Yet identification of the Van Dommelen and Shen process is not automatic even though its structure is known. For example, it will not show up in the vorticity flux through the boundary-layer cross section since the important particle motion occurs near vorticity reversal. On the other hand, it becomes evident in the wall shear and wall pressure only after it starts inducing significant boundary-layer displacement effects, at which time the structure is already firmly established.

An understanding of the process of interaction between the structure and the ambient irrotational flow may facilitate an earlier discovery of the separation process. A first step toward such understanding was recently made by Cowley et al.[20] through the formulation of an appropriate model of interaction, amenable to analysis. The previous interaction models led to quite intractable formulations. It would further be desirable to extend the Van Dommelen and Shen structure to higher order to identify more clearly up to which times the structure describes the flow well, as well as to show its initial effects.

**Origin of the Dynamic-Stall Vortex**

The vortex method allows a meaningful study of a question less readily addressed by other methods: the question of where the shed vorticity originates. The question of the origin is

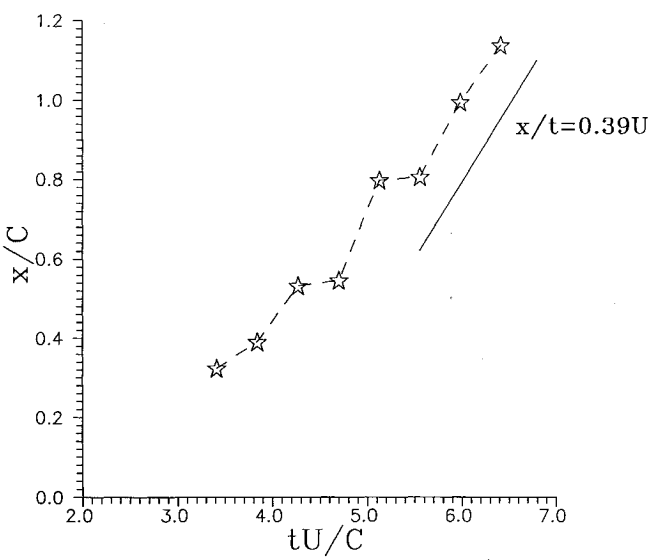


**Fig. 5 Chordwise evolution of the primary vortex.**

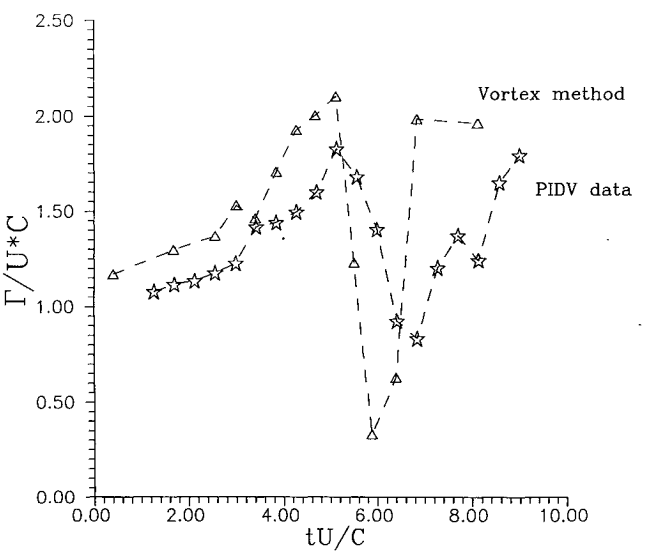


**Fig. 6 Time variation of the upper surface circulation.**

important when effects that convect with the fluid (temperature disturbances, water vapor, vorticity fluctuations due to wall roughness, etc.) influence the vortex. To see how the question of the origin can be resolved, we recall that the vorticity is generated at the surface of the airfoil and diffuses away from it. We can therefore subdivide the surface into segments and color code vortices created at different segments with different colors. Since vortices retain their identity in the computation, vortices originating from a red wall segment remain always red, from a blue segment blue, etc. Then the colors present in any small region of the flow give a qualitative idea about what parts of the wall can influence that region sizably through convective-diffusive processes.

In the example presented here, the airfoil surface is partitioned into six regions: four on the upper surface and two on the lower surface. Vortices generated from these regions, regardless of their sense of rotation, are colored corresponding to the color code assigned to their origins. We could formalize this discrete numerical procedure into a definition of a continuous density function for each color satisfying the same convection-diffusion equation as the vorticity. However, since diffusion constants may vary, only qualitative trends are likely to be of interest, and the described method has the advantage that it gives a picture of how the numerical solution develops.

Figure 7 shows resulting vortex origins at different times. The most important conclusion that can be drawn is that while the main leading-edge vortex may be located above the center of the airfoil, the vorticity in it originates almost totally from the immediate vicinity of the leading edge. Thus manipulation of the vortex through convective disturbances must be done at the leading edge, not at some location immediately below the vortex.

### Local Flow Near the Nose

To arrive at conclusions about the leading-edge stall that have a wider applicability than just for one specific flow, and to extrapolate results to other flows, appropriate models are needed. The Van Dommelen and Shen structure is believed to apply generally, but it only describes the initial development, and current interaction models hardly extend the range of applicability.[20] Models are also needed for times beyond the initial vortex formation. Examples of existing models are descriptions in terms of simplified vorticity mechanics, including the vorticity balance concept[19] and thin airfoil and interaction theories for nearly attached flows. The inviscid similarity solution[14] seems to explain the starting vortices generated at the trailing edge well.

At the leading edge, the extension of the Van Dommelen and Shen structure to significantly later times would be a major step in understanding the total flow. Still, at present it does not yet seem feasible to extend this structure to times significantly beyond separation through conventional interaction theories, since the time scales of subsequent processes become shorter rather than longer.[20] For that reason, subsequent stages must currently be described by full Euler or Navier-Stokes solutions.

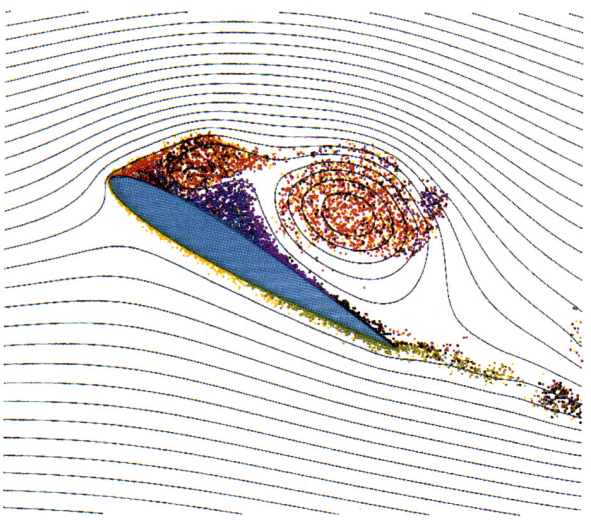

**Fig. 7 Identification of the origin of the dynamic-stall vortex by color-coded point vortices.**

Thus the question becomes whether the solutions of the Navier-Stokes equations can be understood in general terms by means of some simple and general concept. A particularly promising model is that of a thin airfoil, which leads to the notion that to some fundamental level of approximation the flow near the nose can be studied in isolation. In this framework, the formation and shedding of the leading-edge vortex is governed by local processes only. The model can in principle include a Van Dommelen and Shen type initial separation and evolve to a Pullin type fully detached leading edge.

Note that, although such flows have been studied before in terms of boundary-layer solutions, e. g., Smith,[21] our approach is different. We hope to use them to derive valid approximations to solutions of the Navier-Stokes equations, under conditions in which the boundary-layer thickness cannot be ignored compared with the nose radius. In particular, we want to describe global separation of the leading-edge flow.

For conventional airfoils, the flow near the nose resembles flow about a parabola, and the global features merely change the rate of flow around this parabola.[21] Such a flow provides a generalized approximation that does not directly depend on detailed features such as airfoil thickness, camber, geometry, and trailing edge. We can instead include such effects in terms of an effective angle of attack that describes the rate of flow around the nose. Before stall, this rate is proportional to

$$\alpha_e = \tfrac{1}{2}\alpha_c(1+f) - \tfrac{1}{8}\dot{\alpha}(1-f) \tag{5}$$

where $\alpha_c$ stands for the tangent of the angle between the velocity of the midchord point and the chord, with $U$ the component along the chord. The correction factor $f$ accounts for possible circulation around the airfoil. In case the flow is started from rest, theoretically the global circulation should be zero, since the evolution at the nose should be rapid and the trailing-edge vortex is initially very close to the trailing edge. As a result, theoretically $f$ vanishes. At the other extreme, when the evolution of the flow at the nose would be very slow, the global flow could behave quasisteady, and imposition of a Kutta condition would lead to the value $f = 1$.

Near the nose the relevant length scale becomes the nose radius of curvature $r_{le}$. Since this length is small, $0.016C$ for a NACA 0012, the question arises why the airfoil can perform a sizable motion before stall occurs. The solution appears to be merely numerical; in Fig. 8 a typical flow about a parabolic nose is presented: the scaled effective angle of attack $\alpha_e/\sqrt{2r_{le}/C}$ was 2.5, and the Reynolds number based on the nose radius was 79.2. It is seen that it requires a considerable time (measured in nose radii motion) for a clearly discretized vortex to form.

The parabolic nose is a good opportunity to learn some general features of unsteady stall, and work is continuing on it. For the time being we only note that Visbal and Shang[10] suggest using the velocity of the nose of the airfoil as a measure of the stage of evolution of the flow. However, definition (5) is more meaningful for theoretical studies, and their Fig. 9 shows the relevance of Eq. (5) as well as their criterion.

### Repeatability

Some simple numerical experiments showed that the vortex method results at later times are relatively sensitive to the numerical parameters. Since the vortex method will probably describe the inviscid processes and trailing edge vortex well, it seems that the viscous effects may have a significant influence

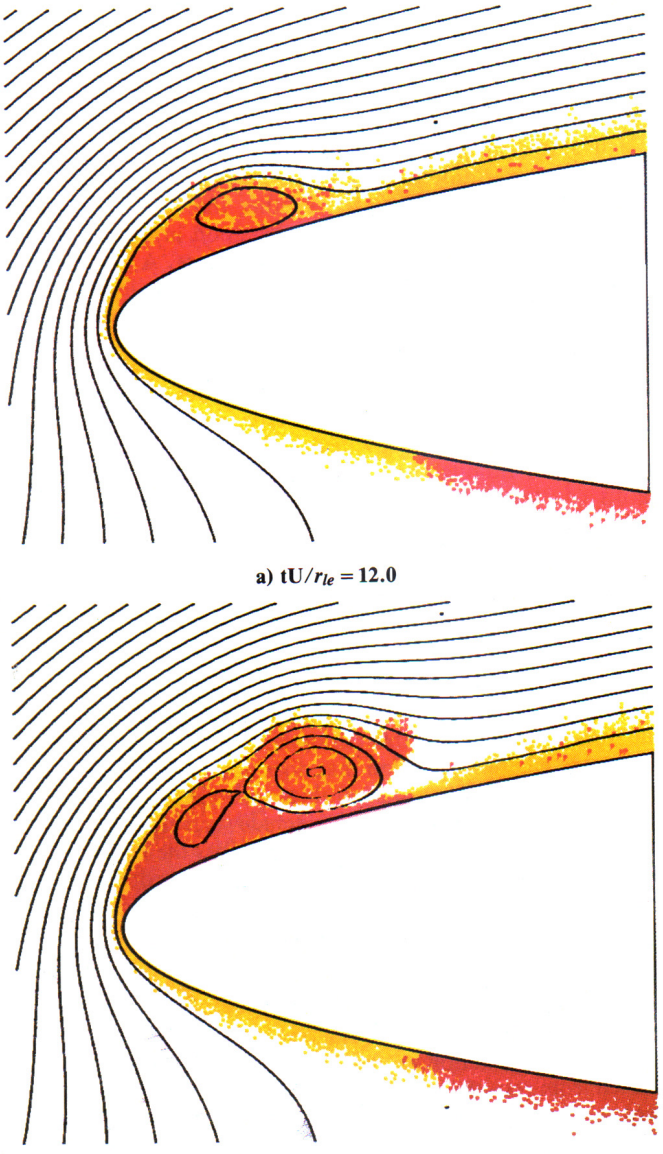


**Fig. 8 Leading-edge flow separation near a parabolic nose; point vortex method.**

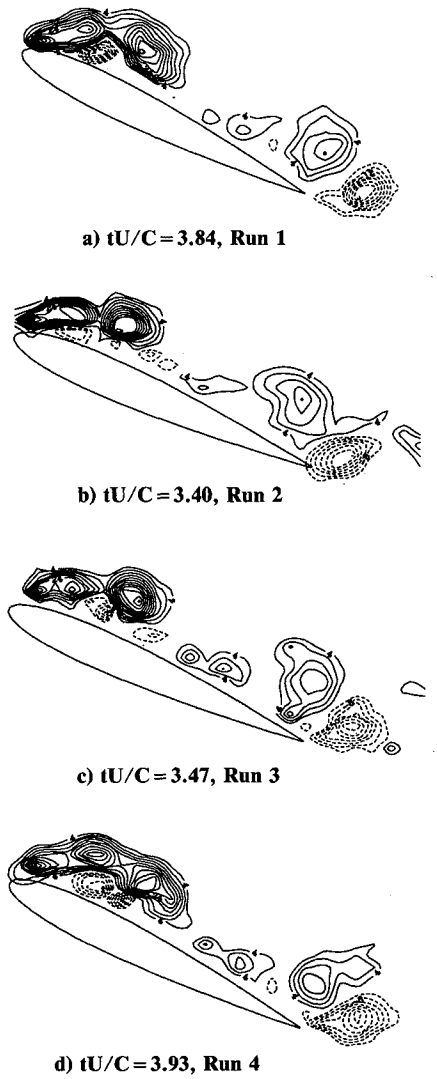


**Fig. 9 Instantaneous vorticity distributions for duplicate experimental runs.**

on leading-edge stall at this Reynolds number. It would be interesting to replace the random walk simulation of the diffusion by a deterministic mesh-free method as proposed by Van Dommelen,[22] since that would allow a systematic sensitivity analysis of the results.

To show the reproducibility of the experiment, four duplicate PIDV data sets are compared. The general features discussed earlier are well preserved in each case. However, there appear to be phase differences between data taken at different runs. Figure 9 illustrates such a comparison by showing the global vorticity fields at approximately the same flow development stage for different runs. The formation of a counter-rotating vortex pair at the trailing edge demonstrates the synchronization of the flow development between runs. Clearly there is a time difference between runs and, more specifically, runs no. 1 and 4 are lagging behind the others. The dimensionless lagging time, $\Delta t U_\infty / C$, is approximately of the order of 0.4. Jumper et al.[23] have reported similar data scatter in their study of the unsteady lift characteristic for an airfoil pitching at constant rate. A phase scatter of the order of $\Delta t U_\infty / C \approx 0.8$ is obtained from their data. The larger time shift is compensated by the lower pitching rate of their experiment.

The magnitude of the variance well exceeds any plausible experimental uncertainty. Clearly, there must be some mechanism that magnifies small differences between individual runs considerably. It seems unlikely to us that at least the initial evolution of the trailing-edge vortex would be so sensitive, but a Kelvin-Helmholtz type instability mechanism during the formation of the main leading-edge vortex could magnify disturbances considerably. Even earlier in the evolution of the flow near the nose the velocity profiles are expected to be very unstable.

If the flow is sensitive due to such instabilities or other mechanisms (viscous instabilities, vortex interactions, wake instability, etc.), either natural or artificial randomness generated during the experiment may be responsible for the inconsistencies between runs. In a wind-tunnel experiment, it can be due to the freestream turbulence or it can result from the sensitive nature of flow separation to laminar-to-turbulent transition. In a water towing tank setup, as in our experiment, residual vorticity fluctuations that remain from previous runs also can result in phase jitter. Consequently, we believe run no. 1 to be the most reliable, and all results in this paper are taken from this run. (Note that, typically, the time intervals between experiments were 5 or more minutes, or until there was no visible sloshing motion in the tank.)

Regardless of its origin, due to the existence of the randomness the interpretation of experiments using a phase-averaging technique could be misleading. This further justifies the importance of using the whole-field PIDV technique in the study

of the unsteady aerodynamic problem. In summary, we feel that it is simply not true that a large number of transient flows with delicate features such as thin vortex sheets are the same as one average flow with "smear-out" features such as thick vortex layers; the later model is not representative of any of the original individual flows.

## Conclusions

The flow past an airfoil pitching up at a constant rate was studied. The results prove the ability of the PIDV technique to provide instantaneous velocity and vorticity fields to high spatial resolution and accuracy for such complex flowfields. At the current stage of implementation, the PIDV method has proven to be quite efficient. For example, it takes approximately 15 min to fully process the entire flowfield with more than 2000 velocity vectors. A discrete vortex, random walk computation was undertaken that complements and confirms our experimental findings. The results establish the fast summation vortex method as a useful tool in studying flows with large-scale unsteady separation.

Under the conditions studied, leading-edge flow separation develops when $\alpha > 20$ deg, and results eventually in a local accumulation of vorticity. The development of the leading-edge vortex dominates the later flow behavior. This vortex grows to a size that is comparable with the airfoil chord and moves downstream. A counter-rotating vortex is released from the trailing edge when the leading-edge vortex comes sufficiently close to it. At about the same time, a complete detachment of the leading-edge boundary layer triggers the airfoil into deep stall.

During the evolution of the leading-edge separation, a ramp-like vorticity structure was observed that was suggestive of a Van Dommelen and Shen separation process. This process takes place before there is a sizable imbalance of net vorticity transport through the boundary layer and is not directly related to production of vorticity. The Van Dommelen and Shen process may be the last stage in the evolution of unsteady stall that can be effectively modified. This aspect warrants further study.

To generalize some flow features, efforts to study the nose in isolation were begun. For the isolated problem, airfoil thickness, camber, and shape may be scaled out, whereas the Reynolds number is rescaled with the nose radius, allowing much higher Reynolds numbers based on the chord to be described. Preliminary results show that it takes a large nondimensionalized time ($\approx 18$) for an individualized vortex to form, which explains why unsteady stall does not take place very quickly, after a few nose radii motion, even when the static stall angle is well exceeded.

The nonperiodic nature and low reproducibility of the studied flow favors the use of a whole-field PIDV as opposed to, for example, phase averaging. Indeed, the instantaneous flow will not be close to an averaged flowfield, and to understand the instantaneous fluid mechanics truly, we must take account of that fact.

## Acknowledgments

This work is supported by the Air Force Office of Scientific Research under Contract AFOSR F49620-89-C0014. The authors acknowledge the support of the Supercomputer Computations Research Institute and the Florida State University through use of their computer facility.

## References

[1]McCroskey, W. J., "Unsteady Airfoils," *Annual Reviews of Fluid Mechanics,* Vol. 14, 1982, pp. 285–311.

[2]Visbal, M. R., "On Some Physical Aspects of Airfoil Dynamic Stall," *Proceedings of the International Symposium on Nonsteady Fluid Dynamics,* edited by J. A. Miller and D. P. Telionis, FED Vol. 92, American Society of Mechanical Engineers, New York, 1990, pp. 127–147.

[3]Francis, M. S., and Keesee, J. E., "Airfoil Dynamic Stall Performance with Large-Amplitude Motions," *AIAA Journal,* Vol. 23, No. 11, 1985, pp. 1653–1659.

[4]Shih, C., "Unsteady Aerodynamics of a Stationary Airfoil in a Periodically-Varying Free-Stream," Ph.D. Thesis, Univ. of Southern California, Dept. of Aerospace Engineering, Los Angeles, CA, Aug. 1988.

[5]Lourenco, L., and Krothapalli, A., "Particle Image Velocimetry," *Lecture Notes in Engineering: Advances in Fluid Mechanics Measurements,* edited by M. Gad-el-Hak, Springer-Verlag, Berlin, 1989, pp. 128–199.

[6]Van Dommelen, L. L., "Lagrangian Techniques for Unsteady Flow Separation," Forum on Unsteady Flow Separation, *Proceedings of the 1987 ASME Applied Mechanics, Bioengineering, and Fluids Engineering Conference,* FED Vol. 52, American Society of Mechanical Engineers, New York, 1987, pp. 81–84.

[7]Van Dommelen, L. L., and Rundensteiner, E. A., "Fast Solution of the Two-Dimensional Poisson Equation with Point-Wise Forcing," *Journal of Computational Physics,* Vol. 83, No. 1, 1989, pp. 126–147.

[8]Smith, P. A., and Stansby, P. K., "An Efficient Surface Algorithm for Random-Particle Simulation of Vorticity and Heat Transport," *Journal of Computational Physics,* Vol. 81, 1989, pp. 349–371.

[9]Wu, J. C., "Theory for Aerodynamic Force and Moment in Viscous Flows," *AIAA Journal,* Vol. 19, No. 4, 1981, pp. 432–441.

[10]Visbal, M. R., and Shang, J. S., "Investigation of the Flow Structure Around a Rapidly Pitching Airfoil," *AIAA Journal,* Vol. 27, No. 8, 1989, pp. 1044–1051.

[11]Sears, W. R., and Telionis, D. P., "Boundary Layer Separation in Unsteady Flow," *SIAM Journal of Applied Mathematics,* Vol. 23, No. 1, pp. 215–235.

[12]Shen, S. F., "Unsteady Separation According to the Boundary-Layer Equation," *Advances in Applied Mechanics,* Vol. 18, Aug. 1978, pp. 177–219.

[13]Williams, J. C., III, and Stewartson, K., "Flow Development in the Vicinity of the Trailing Edge on Bodies Impulsively Set into Motion, Part 2," *Journal of Fluid Mechanics,* Vol. 131, 1983, pp. 177–194.

[14]Pullin, D. I., "The Large Scale Structure of Unsteady Self-Similar Rolled-Up Vortex Sheets," *Journal of Fluid Mechanics,* Vol. 88, Oct. 1978, pp. 401–430.

[15]Van Dommelen, L. L., and Cowley, S. J., "On the Lagrangian Description of Unsteady Boundary Layer Separation, Part 1: General Theory," *Journal of Fluid Mechanics,* Vol. 210, Jan. 1990, pp. 593–626.

[16]Tietjens, O. K. G., *Fundamentals of Hydro- and Aeromechanics,* Dover, New York, 1957.

[17]Harvey, J. K., and Perry, F. J., "Flowfield Produced by Trailing Vortices in the Vicinity of the Ground," *AIAA Journal,* Vol. 9, No. 8, 1971, pp. 1659–1660.

[18]Didden, N., and Ho, C. M., "Unsteady Separation in a Boundary Layer Produced by an Impinging Jet," *Journal of Fluid Mechanics,* Vol. 160, Nov. 1985, pp. 235–256.

[19]Reynolds, W. C., and Carr, L. W., "Review of Unsteady, Driven, Separated Flows," AIAA Paper 85-0527, Jan. 1985.

[20]Cowley, S. J., Van Dommelen, L. L., and Lam, S. T., "On the Use of Lagrangian Variables in the Descriptions of Unsteady Boundary-Layer Separation," *Philosophical Transactions of the Royal Society of London,* Series A, Vol. 333, No. 1631, 1990, pp. 343–378.

[21]Smith, F. T. "Concerning Dynamic Stall," *Aeronautical Quarterly,* Vol. 33, Nov./Dec. 1982, pp. 331–352.

[22]Van Dommelen, L. L., "Some Experiments on a Vortex Redistribution Method," American Mathematical Society Regional Meeting, Hoboken, NJ, Oct. 21–22, 1989; also Fluid Mechanics Research Lab., Florida State Univ., Rept. FMRL-TR 3, Tallahassee, FL, Aug. 1989.

[23]Jumper, E. J., Schreck, S. J., and Dimmick, R. L., "Lift-Curve Characteristics for an Airfoil Pitching at Constant Rate," *Journal of Aircraft,* Vol. 24, No. 10, 1987, pp. 680–687.